Demonstration of inscription and ablation of phase masks for the production of 1st, 2nd and 3rd order FBG gratings using a femtosecond laser

Graham N. Smith*[a], Kyriacos Kalli[b], Ian Bennion[a], Kate Sugden[a]

[a]Photonics Research Group, Aston University, Birmingham, B4 7ET, UK;
[b] Nanophotonics Research Laboratory, Cyprus University of Technology, Limassol, Cyprus

ABSTRACT

We present to the best of our knowledge the first example of femtosecond laser inscription/ablation of phase/amplitude masks for the demonstrated purpose of inscribing Bragg gratings in optical fibers. We show that the utilization of a femtosecond laser for the mask production allows for great flexibility in controlling the mask period. The masks are used to produce 1st, 2nd and 3rd order fiber Bragg gratings (FBGs) in SMF-28. The work demonstrates the proof of concept and flexibility for the use of femtosecond lasers for the rapid prototyping of complex and reproducible mask structures. Our inscription studies are augmented by considerations of three-beam interference effects that occur as a result of the strong zeroth-order component that is present in addition to higher-order diffraction components.

Keywords: Phase masks, Femtosecond laser, inscription, laser-material interaction, fiber Bragg gratings, Talbot effect

1. INTRODUCTION

Phase masks have been used for the production of fiber gratings since Bennion *et al* first demonstrated their use to produce side etched gratings in 1986[1]. In 1989Meltz *et al*[2] showed that gratings could be directly written into fiber using an interferometric approach involving a UV lasing exposure. However, it was the combination of these two approaches – UV writing through a phase mask by Hill *et al* in 1993[3], that provided the necessary momentum for fiber Bragg gratings to become a mass produced commodity item.

The phase masks utilized in grating inscription are used to spatially modulate the UV-writing beam and are typically surface relief structures, with the gratings most often etched in fused silica (because of its low absorption of UV wavelengths) either through a holographic or electron-beam process. One of the advantages of electron-beam lithography over the holographic technique is that complicated patterns, such as quadratic chirps and Moire patterns can be written into the mask's structure. However, lithographically induced phase masks usually are generated by stitching together small subsections (400μm x 400μm) of periodic corrugations on the mask substrate to fabricate large phase structures. An error in the precise positioning of the various subsections results in what is commonly referred to as stitching error[4]. Holographically induced phase masks, on the other hand, have no stitch error. The masks act as precision diffraction gratings that upon irradiation by a monochromatic source divide the light evenly between two or more orders. These created orders interfere in the area behind the phase mask where they overlap and this interference pattern is recorded in the fiber to create the FBG.

The incident and diffracted beams follow the general diffraction equation,

$$\Lambda_{pm} = m \frac{\lambda_w}{\sin \varphi_m - \sin \varphi_i}$$

where Λ_{pm} is the mask period, φ_i is the incident angle, φ_m is the angle of the diffracted order, and λ_w is the wavelength of the writing UV beam, and m is the diffraction order from the mask. The m=0 order corresponds to the transmitted beam.

*smithgn@aston.ac.uk; phone (+44) 0121 204 3496; fax (+44) 0121 204 3682; http://www.ee.aston.ac.uk/research/prg/

In the simple case where the incident UV radiation is normal ($\varphi_i = 0$), the positive and negative orders have equal diffraction angles. The interference formed between the beams of various orders ($m = \pm 1, \pm 2, \ldots$) are used to generate the fringe pattern that inscribes a Bragg grating in optical fibers. Typical masks use either the +1/-1 (or 0/-1) orders optimized to diffract light equally and maximally into the plus and minus first orders (or zero and minus first order). Manufacturers optimize the mask designs to suppress additional orders where possible. The fringe pattern created by the interference of two orders, with maximal suppression of all other orders, has half the phase of phase mask period.

$$\Lambda_{fringe} = \frac{\Lambda_{pm}}{2}$$

Whilst most commercial development of this technology has used phase mask technology another approach was proposed by Mihailov et al in 1994[5]. In this instance an amplitude mask, with line spacings of between 5 and 120 μm was imaged to produce higher order gratings. The advantage of this approach is that the mask structure can be easily and quickly manufactured without the need for lithographic technologies but first order gratings are difficult to make and the imaging optics required is quite costly.

In this work we present the first example of masks written with point by point femtosecond inscription. These masks have been used to fabricate grating structures that can be written in fiber and doped substrates. The nature of the mask fabrication method also demonstrates a potential for swift adaptation and tuning to meet specific applications through two routes; the manipulation of coding the motion of the sample relative to the inscribing laser beam, and control of the parameters for both the host material and inscribing laser.

2. EXPERIMENTAL WORK
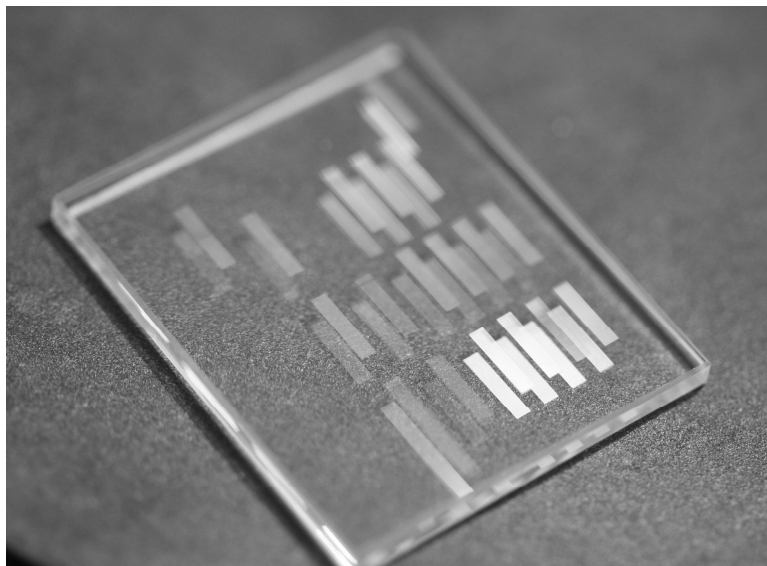
2.1 Fabrication of the masks

Fig 1. Image of a series of fs written patterns

A number of diffraction patterns were inscribed into the bulk volume of glass samples with a variety of periods. Figure 1 shows a set of patterns written in such a glass substrate. The substrates used were made of pure fused silica supplied by Ibsen Photonics. The samples had dimensions of 30x25x2 mm and were chosen for the flatness and optical quality of the UV grade fused silica. The uniformity of the substrate was found to be critical in the reproducibility of the masks. This

glass was known to be highly transmissive in the wavelength region from 193nm to 693nm, which is a fundamental requirement for the use of these masks in the production of FBG. In order to exploit the photosensitive nature of the optical fibers for Bragg grating inscription, the fibers are illuminated typically at laser wavelengths in the UV or near UV.

The laser used to write the patterns in the silica substrates is an Amplitude Systemes s-pulse HP laser that produces sub 500fs pulses at a wavelength of 1026nm and average powers of 550mW. The laser is incorporated into an Oxford Lasers micromachining system that consists of four air bearing stages mounted on a large granite bed for stability. The system incorporates on the move optical power control and a vision system for high accuracy alignment. The motion control system is based on Aerotech ABL 1000 air bearing stages. These are controlled by a dedicated A3200 Aerotech control unit, from which the stages are controlled by the G-code used for CNC programming of the motion. The repeatability and precision of these stages allows this work to be carried out with minimal stitch errors and with the accuracy required to obtain the precise lines written in the fused silica substrates. The high precision multi-axis high resolution air bearing stages have the sub-nm alignment accuracy critical for writing these structures.
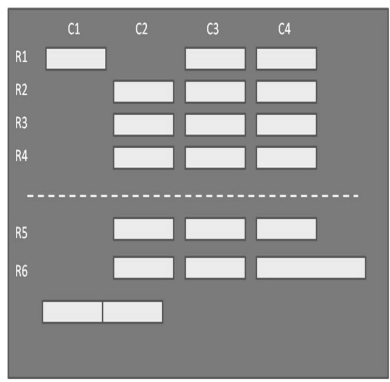
The pure fused silica samples were mounted on the multi-axis stages using a specially designed jig that securely clamps the sample on all sides both top and bottom whilst not creating stress or warping the substrate. The sample was also secured such that it was perpendicular to the incident femtosecond beam. Low stress mounting of the samples was critical as the inscription mechanism is based on non-linear absorption of the focused femtosecond laser light, hence it is important to avoid unwanted effects from non-linear interactions that would change the uniformity of the written structure that is dependent on the direction of the inscription. The inscription laser polarization was chosen to be circular, in this way the dependence on the relation between write direction and polarization state is largely negated. Although not truly optimized it enables the total write process to be partially optimized no matter the direction of stage travel. This also enables the total write time to be kept shorter as there is no optimization based on the direction of the sample, travel or polarization state that would otherwise take additional time.

The inscription lens used was a Mitutoyo x100 NIR lens. This was chosen as it provides a long working distance with a high NA thus generating a small and highly accurate focal spot that the structures written required. The accurate nature of the spot through the sample due to the large NA and working distance are critical to the direct write nature of the work.

The air bearing stage system was controlled through programming in G-code. The coding was written to enable flexible motion control producing typically mask patterns of 5x1mm at a range of depths and pitches. The depth of the written structures varied from the surface to a depth of 150 µm . This was carefully controlled using a piezo lift stage after having identified the position of the substrate top surface. The row R1 was written at the surface, R2 at a depth of 75 µm, R3 at 100 µm and R4 at 150 µm. The pitch of the masks was chosen to be 1060nm, 2120nm and 3180nm. Columns C1-C4 represent different written periods as described in the figure below. This was with the aim of the masks being used to write 1st, 2nd and 3rd order gratings at the C-band wavelength range for use with SMF-28 fiber. On the substrate described here a set of 18 mask patterns were written with the periods and energy levels as shown in the table below. The second set of mask patterns, shown below the dotted line in the figure below, were written in order to investigate the effect of energy levels on the inscription process and subsequent grating quality. The energies used range from 1 µJ to 8 µJ, the energies were measured at the objective lens and were varied by the use of an external attenuator unit in the system. The parameter for the energy per pulse is shown as Epp in the table below.

Table 1. (a) Table showing the inscription parameters used in production of the phase masks (b) schematic of the substrate

	C1	C2	C3	C4	
R1	Λ=1060nm Epp=4µJ		Λ=2120nm Epp=4µJ	Λ=3180nm Eppr=4µJ	
R2		Λ=1060nm Epp=4µJ	Λ=2120nm Epp=4µJ	Λ=3180nm Epp=4µJ	
R3		Λ=1060nm Epp=4µJ	Λ=2120nm Epp=4µJ	Λ=3180nm Epp=4µJ	
R4		Λ=1060nm Epp=4µJ	Λ=2120nm Epp=4µJ	Λ=3180nm Epp=4µJ	
R5		Λ=2120nm Epp=1µJ	Λ=2120nm Epp=2µJ	Λ=2120nm Epp=4µJ	
R6		Λ=2120nm Epp=6µJ	Λ=2120nm Epp=8µJ	Λ4000nm Epp=4µJ	

The laser was optimized and then set to operate at 100 kHz repetition rate. This was experimentally found to be the optimum repetition rate producing the most well-defined and smooth lines whilst keeping the overall write time low. A laser energy of 4µJ was found to produce reliable and clear lines for which the inscription process was found to produce the most consistent results.

As with the power levels and repetition rate the translation speed of the stages was optimized. It was found that 1mm/s gave the best results in terms of pattern quality. The code was adjusted such that the raster (the rectangular formation of a series of parallel scanning lines) function written allowed the stages to operate accurately with negligible error based on positional error originating from the acceleration and deceleration of the stages. This was optimized and the stages tuned to give the accuracy required for the pitch and line quality required to produce the masks. The stage speed was also adjusted as to avoid any issues with overwriting and also to adjust the overall write time.

The nature of the line by line inscription allows for the specific design parameters to be optimized quickly and adapted to meet any specific requirements. Although the bulk of the masks made have been optimized for use with silica optical fiber other masks have been produced that were optimized for use with polymer planar and fiber samples. These have been designed to work at different wavelengths, both of the laser illumination and of the grating produced, to be appropriate for the transmission spectra of polymer fibers. This is a simple example of the ease of adaptation; more complex structures can also be produced via adjusting the coding and parameter space used. This flexibility is one of the key advantages of this process and has the potential to give a broad range of masks dependent only on the optimization and parameter space of the inscription.

The nature of these masks, being written inside the substrate, also provides other advantages over the cleaning procedures of a standard commercially available phase mask. Typically the regular cleaning of these masks involves the use of semiconductor grade acetone and clean room environments and at no point can contact with the mask be made, whilst the full cleaning process requires the use of sulphuric acid and is often carried out by sending the masks back to the supplier. In sharp contrast the cleaning of the masks produced here involves only the use of pure methanol or acetone and optical tissue to draw across the sample. This makes the running cost and handling of these masks much easier, more robust and significantly cheaper.

The total write time for producing a mask runs from between 2hrs 20 minutes, to at its maximum, a time of 3hrs. This is the time taken to produce masks of 5x1mm and the difference reflects the increased number of lines of inscription for masks of a shorter pitch length. These write times may well be shortened with some changes to the inscription procedure through further optimization of the air-bearing stage coding The time taken to adapt the pitch, power, dimensions and other parameters is negligible as this has been built into the code so that it can easily be varied. More complex desired masks such as phase shifted and chirped both of which have been written using the same techniques. The ease of

variability and speed of production exceeds that of the commercially available masks which are often multi-step process production lines that are less easily adapted.

2.2 Characterization of masks

The masks were characterized in two different ways (a) by using the diffraction of a helium neon laser, by (b) by using a transmission microscope that incorporated a QPm measurement. The reason for using both approaches is to check the measured parameters against each other and to be certain that the Talbot effect is not giving false readings (this will be discussed later in the paper).

The light transmitted through the masks was measured using both a helium neon laser and a CW ultraviolet laser operating at 244nm. The transmission measurements with the HeNe laser showed no dependence on the mask pitch or the inscription femtosecond laser energy. However, the transmission of the UV laser through the masks changed, showing a decline in transmitted power for masks written with increasing femtosecond inscription pulse energies, varied from 2 to 4 to 8µJ.

By measuring the angle of diffraction for the different diffracted mask orders it was possible to confirm the period of the mask. Table 2 shows the diffraction angles of the orders measured and the phase mask periods calculated using the standard diffraction equation: $m\lambda = d\sin\theta$, where m is the diffraction order, λ is the wavelength of the incident light; d is the grating period and θ is the diffraction angle. Both patterns were fabricated using a pulse energy of 4µJ. From these results it can be seen that there is good agreement with the programmed grating periods and the values calculated from the measured diffraction angle. The majority of the diffracted energy lies in the zeroth order with the higher orders having diffraction efficiencies that vary between 1 and 5%.

Table 2. Measurements of diffraction angle

Set mask period – 4µm			Set mask period – 2µm		
Order	Diffraction angle (°)	Calculated period	Order	Diffraction angle (°)	Calculated period
+3	29.2	3.89			
+2	18.35	4.02	+2	34.2	2.25
+1	9.29	3.92	+1	18.8	1.96
-1	9.54	3.82	-1	18.8	1.96
-2	18.82	3.92	-2	34.3	2.25
-3	29.61	3.93			
Average period from measurements: 3.923µm			Average period from measurements: 2.104µm		

Using a transmission microscope the structure of the masks could be clearly seen and measured. Figure 2 shows the written mask structure as seen when viewed with a Zeiss Axiomicroscope using a x100, 1.4 NA oil immersion DIC lens. The pattern was designed to have a period of 1060nm pitch and this is shown to be approximately the case (errors in the measurement based upon judging the edge of the written structure make it difficult to get an exact measurement). This pattern was written at a depth of 75µm at 1mm/s translation velocity (in the vertical plane), with 4µJ per pulse at a repetition rate of 100kHz. The plot next to the figure shows the measurement of relative phase change across part of the written structure. This was processed using the Quantitative Phase-amplitude Microscopy (QPm) version 2.0 IATIA LTd, Australia software[67]. This relies on phase contrast techniques to separate and quantify the relationship of phase and intensity of the image. The algorithm used in the software allows phase maps to be calculated from images captured from standard bright field microscopy. The technique allows calculation of relative phase change (radians) which is dependent

on the phase change created by the refractive index change and volume as compared to the surrounding media. Here we use it to demonstrate the clear phase contrast between the written structures and the unwritten areas. The peaks represent the inscribed structures as having a positive index change.
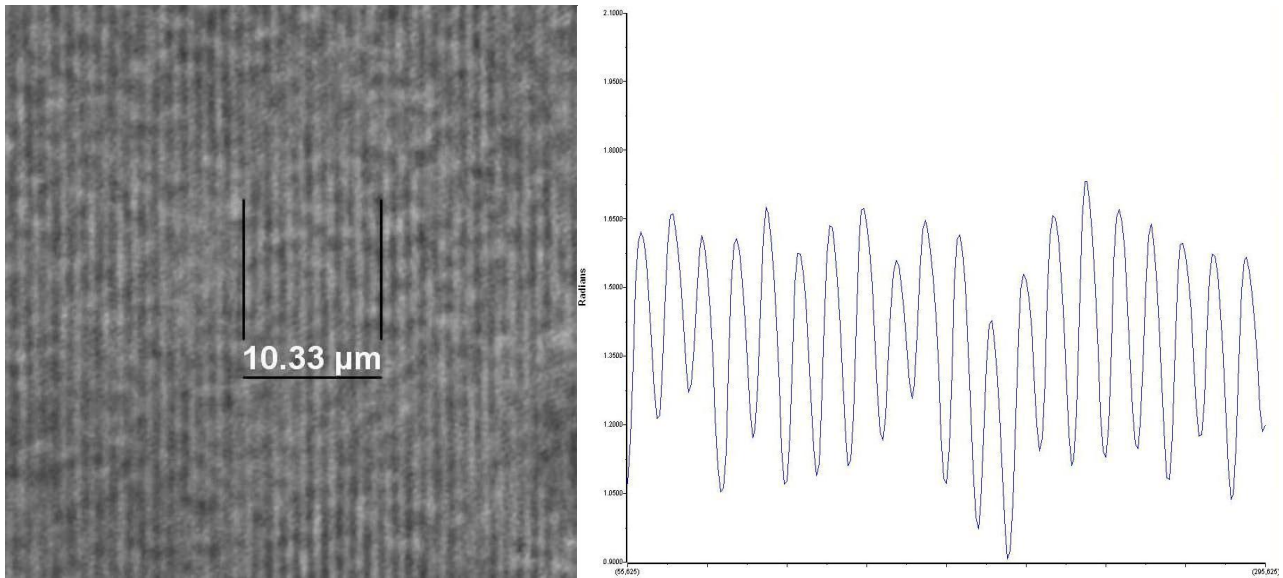

Fig 2. (a) Microscope image of the area C2 R2. The image shows the lines of inscription written with the laser (b) Phase map of 2nd order mask taken over a length of 20 μm.

Figure 3(a) shows a phase mask written at a pitch of 2120nm at a depth of 75μm with a pulse energy of 6μJ per pulse at 1mm/s translation speed and at 100kHz repetition rate. Figure 3(b) next to it shows that over the same distance measured there are half the number of written structures in the same distance, as compared to figure 2(b), leading to the creation of a 4th order phase mask.
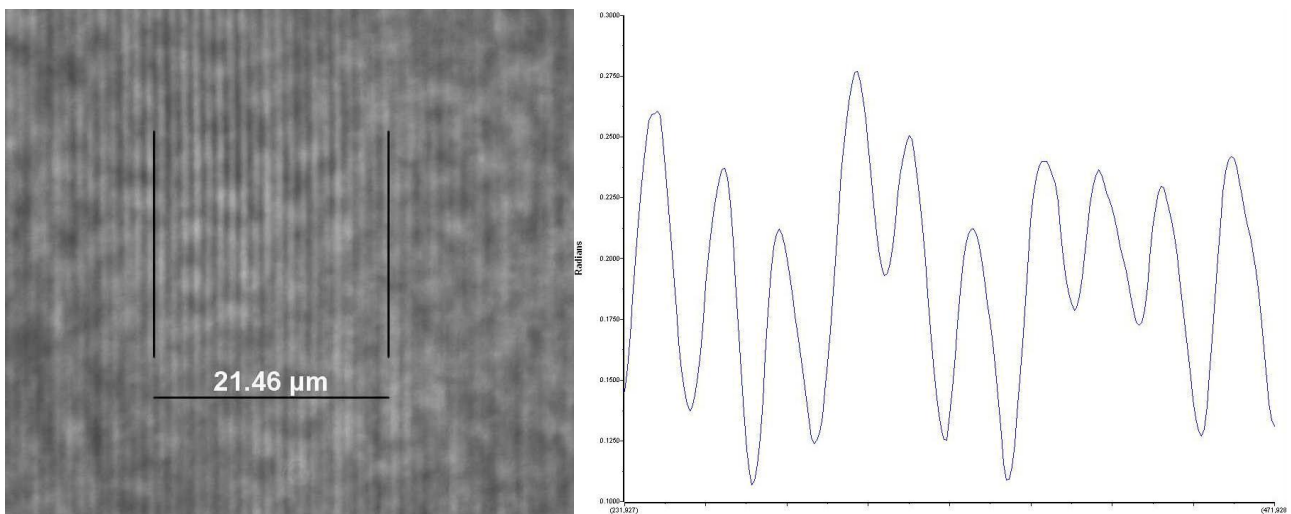

Fig 3. (a) Microscope image of the area C2 R6. The image shows the lines of inscription written with the laser (b) Phase map of 4th order mask taken over a length of 20 μm.

2.3 Fabrication of fiber Bragg gratings

Fiber Bragg gratings were fabricated using all of the masks produced, with varying degrees of success, in hydrogen loaded photosensitive fiber. The laser used to write the FBGs was a Coherent SabreFRED laser which operates CW at a wavelength of 244nm. The system was set up in a conventional manner with the fiber located immediately behind the mask. In this case there was little concern as to whether the fiber came into contact with the mask, which would certainly not be the case with a far more delicate, conventionally produced mask. The laser power was set to 100mW which resulted in approximately 80mW being incident on the fiber. It was possible to fabricate gratings with all inscribed mask structures in the first set of patterns. However, the mask that had a period of 1060nm , inscribed using 4uJ pulses produced the highest quality gratings. Typically gratings with 30dB transmission losses were observed after six consecutive 5mm scans at a velocity of 0.1mm/s. The bandwidth of the 5mm gratings were about 0.18nm and the sidelobes were reasonable symmetrical. There was not a great deal of difference observable between the gratings made with the patterns at different depths.
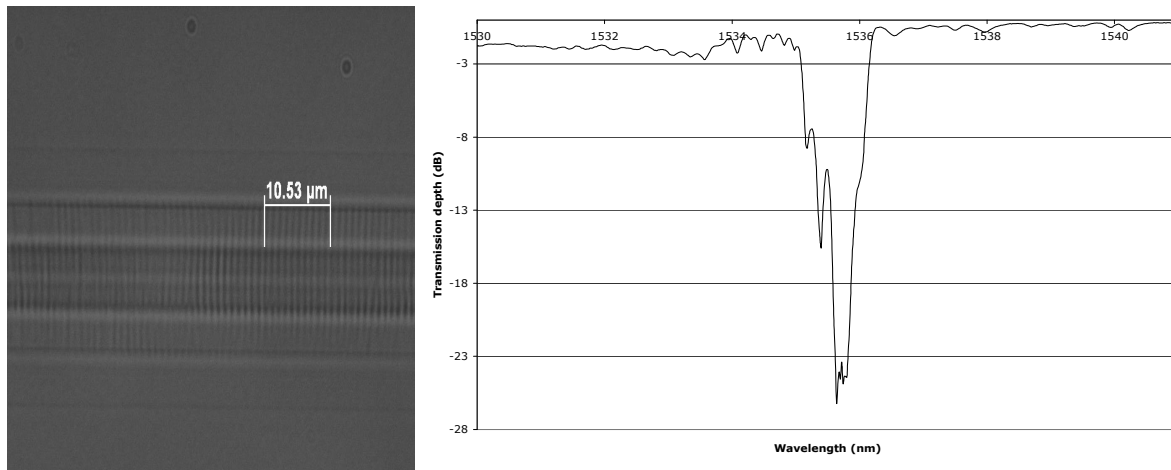

Fig. 4. (a) Microscope image of grating written with 1060nm pitch mask (b) corresponding spectra profile of the grating.

Figure 4 (a) shows a microscope image of a grating created in photosensitive fiber from a mask of 1060 nm at a depth of 100μm depth. Also shown (Figure 4 (b)) is the transmission profile of a 2nd order grating made with six consecutive scans of the this mask each at 0.1mm/s, the mask was written at a depth of 75 μm with a period of 1060nm at an energy of 4 μJ per pulse. This grating reached a maximum transmission depth of 25dB. Strong sidelobes can be seen on the short wavelength side due to the fact that the grating was not apodized.
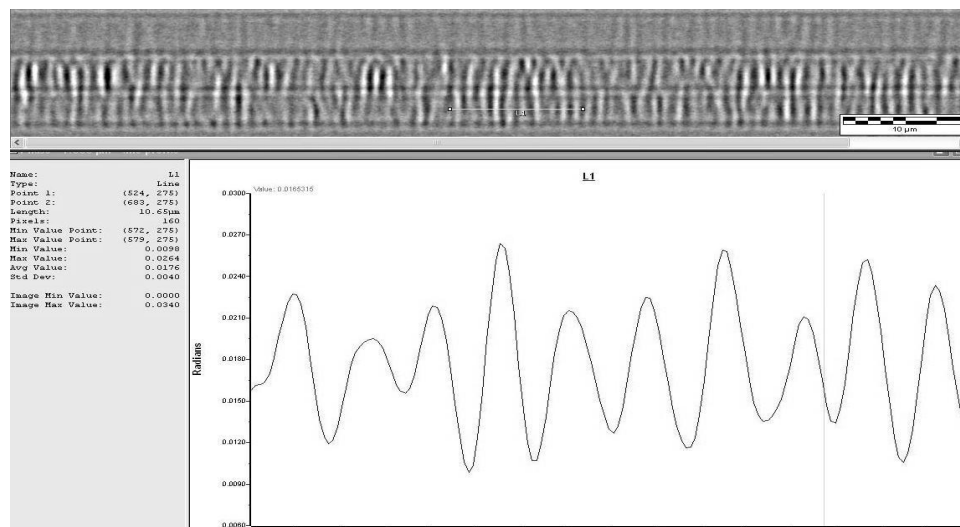

Fig. 5. A QPm Phase contrast map along the grating structure that had been written in the photosensitive fiber.

The results demonstrate the nature of the phase contrast profile inscribed when illuminated using the inscribed mask. They show that the feature has an inscribed period of 1.06μm and is as such a 2nd order grating in the 1550nm band.
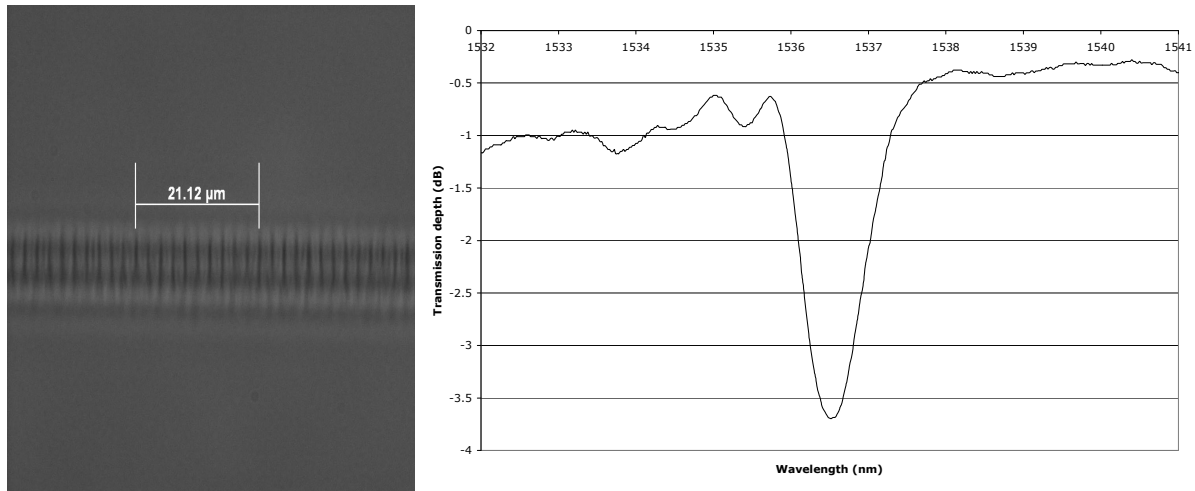

Fig. 6. (a) Microscope image of grating written with a 2120nm pitch mask (b) corresponding spectra profile of the grating.

Fig 6 (a). shows a microscope image of a grating in the core of some photosensitive fiber produced using a mask written at 75μm depth at 2120 nm pitch. As before the grating was made using a scanning UV beam with an incident power of 85mW at 244nm in hydrogen loaded photosensitive fiber. The 4th order grating was fabricated with seven consecutive scans of the fiber each at 0.1mm/s. Figure 6 (b) shows the transmission profile of the grating which reached a maximum transmission loss of 3.7dB.
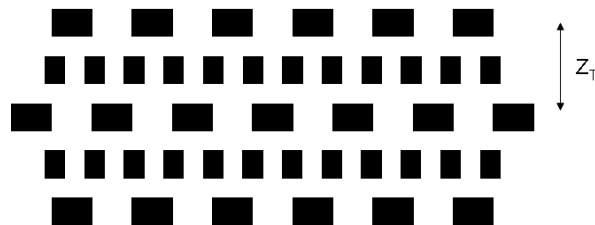
2.4 Discussion of the Talbot Effect

Fig. 7. A schematic showing the definition of the Talbot length, Z_T, used in this paper. In this definition it is taken to be the distance between two planes of the same period although the phase is different.

The interpretation of the microscopic images requires a certain amount of care because of the Talbot effect, which is illustrated in Figure 7. This is a near field diffraction effect seen when a plane wave passes through a periodic structure. It causes the resulting wavefront to be replicated periodic at a separation Z_T given by:

$$Z_T = \frac{a^2}{\lambda}$$

where a is the period of the grating (out of phase spacing) and λ is the wavelength of incident light.

Furthermore a second pattern is generated halfway between these locations that has half the spatial period of the original structure making it appear as if you have written a structure with double the frequency. Further higher frequency patterns are also generated between these points. This is illustrated by Figure 8 where two different microscope images of the same 4 micron pattern are seen where the sample has been translated by 6 microns between the two images.
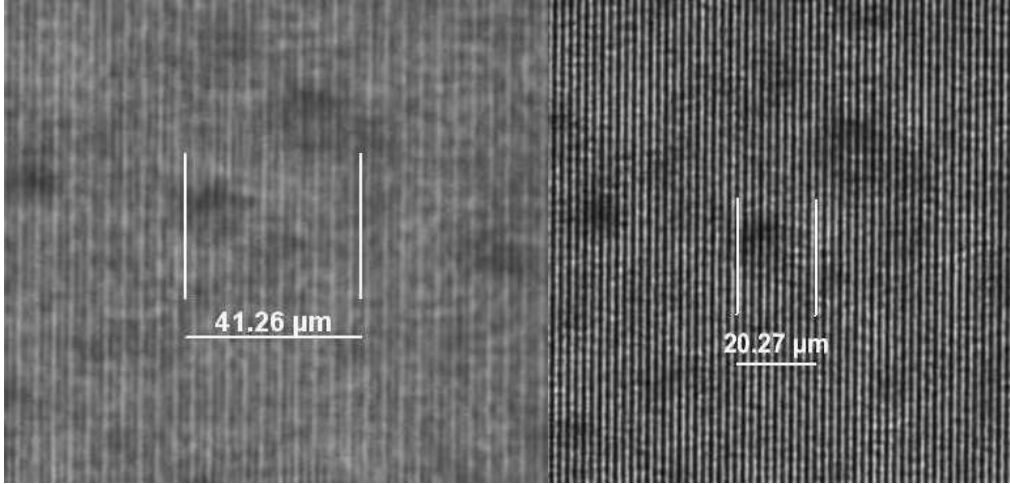
Fig. 8. (a) A microscope image of the 4μm period mask (b) microscope image of double the frequency of the same 4μm mask

Assuming a 500nm illumination of the mask the Talbot distance for the 1.06 μm, 2.12 μm, 3.18μm is 2.25 μm, 8.99 μm and 20.2 μm respectively. For the short period structures this effect tends to add noise to the measurements however with the larger periods the higher frequency images can be clearly seen. Consequently, it is important to cross check the periods measured with the microscope with measurements of diffraction angles for an incident laser beam.

With regard to the inscription of the Bragg gratings using the femtosecond inscribed masks, one needs to consider the effect that the zeroth-order has on any interference pattern that is generated by the mask. This is essentially three-beam interference that results between the non-zero suppression of the zeroth-order with the different diffracted order pairs. Higher order contributions are ignored as they can be minimized by increasing the spacing between the fiber and the mask. The effect of a significant zeroth order contribution on FBG inscription using a phase mask has been analyzed by Dyer et al[8] and by Xiong et al[9]. We use the aforementioned mathematical descriptions to give an indication of the characteristics of the field distribution. We will consider, for the sake of clarity, the interference effects between the ±1 orders and the zeroth order, for which the intensity distribution is given by;

$$ I_{0,\pm 1} = 4 \left[C_1^2 \cos^2 \left(\frac{2\pi x}{\Lambda_{pm}} \right) + C_0^2 + 2C_0 C_1 \cos \left(\frac{2\pi x}{\Lambda_{pm}} \right) \times \cos \left(\frac{2\pi z \left(1 - \sqrt{1 - \left(\lambda_{UV} / \Lambda_{pm} \right)^2} \right)}{\lambda_{UV}} \right) \right] $$

Where C_0 is the amplitude of the electric field of the zeroth order, C_1 for the first order diffraction, and λ_{UV} the UV inscription wavelength. When there is no power in the zeroth order the intensity distribution arises from the first term, being oscillatory in the x-direction with a spatial period of half the phase mask and without variation on the z-axis. The second term is constant and associated with the non-zero contribution of the zeroth order, reducing the fringe contrast of the first term. The third term indicates the interaction between the zeroth and first orders beams that has contribution along the x- and z-axes, with a period Λ_z, given by

$$ \Lambda_z = \frac{\lambda_{UV}}{1 - \sqrt{1 - \left(\lambda_{UV} / \Lambda_{pm} \right)^2}} $$

This equation is equivalent to $2Z_T$, as defined above, and gives the same result for the Talbot distance, given the inscription laser wavelength and mask period. The effect of the non-zero zeroth-order on the interference fringes of the Bragg grating is shown in Figure 9. The figure clearly shows how the presence of the zeroth order modifies the expected fringe pattern producing a spacing equal to the mask period, which in turn leads to the observed, strong, second-order Bragg gratings.
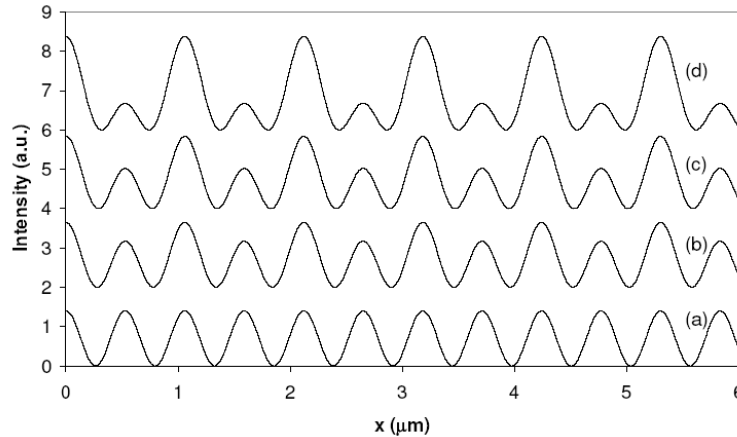

Fig. 9. Intensity distribution along the x-axis at z = 0 for different contributions of the zeroth-order. (a) 0%, (b) 1%, (c) 3% and (d) 13%.

3. CONCLUSIONS

In summary we present to the best of our knowledge the first example of femtosecond inscription/ablation of masks used to produce 1st, 2nd and 3rd order fiber Bragg gratings (FBGs) in SMF-28. The work demonstrates the proof of concept and flexibility for the use of femtosecond lasers to make complex and reproducible masks. This approach to fabricating masks enables the patterns to be below the surface which is helpful in the protection of the tooling and reproducibility of gratings due to positioning variations.

One does need to account for the effect of the non-zero contribution of the strong zeroth-order component that is present in the transmission characteristics of the mask and that modifies the ideal, anticipated interference pattern typically used for Bragg grating inscription. Hence when using the femtosecond inscribed masks for Bragg grating inscription we are inscribing second order Bragg gratings instead of a conventional first order Bragg grating. This is not in itself a major drawback, but pertains from the fact that we have yet to control the effective laser induced "etch-depth" of the mask and its relation to the UV wavelength used for the Bragg grating inscription. This is under development and we anticipate far greater diffraction efficiencies once this issue has been resolved.

3.1 Acknowledgments

REFERENCES

[1] Bennion, I., Reid, D. C. J., Rowe, C. J. and Stewart, W. J., "High reflectivity monomode-fiber grating filters", Electronics Letters, 22, 341- (1986).

[2] Meltz, G., Morey, W. W. and Glen, W. H., "Formation of Bragg gratings in optical fibers by transverse holographic method", Optics Letters, 14, 823- (1989).

[3] Hill, K. O., Malo, B., Bilodeau, F., Johnson, D. C. and Albert, J., "Bragg gratings fabricated in monomode photosensitive optical fiber by UV exposure thourgh a phase mask", Applied Physics Letters, 62 (10), 1035- (1993).

[4] Albert, J., Th´eriault, S., Bilodeau, F., Johnson, D. C., Hill, K. O., Sixt, P. and Rooks, M. J., "Minimization of phase errors in long fiber Bragg grating phase masks made using electron beam lithography", IEEE Photon. Technol. Lett., vol. (8), pp. 1334-1336 (1996).

[5] Mihailov, S. J., Gower and M. C., "Recording of efficient high-order Bragg reflectors in optical fibers by mask image projection and single pulse exposure with an excimer laser", Electronics Letters, 30, (9), 707-708(1994)

[6] Barone-Nugent, E. D., Barty, A. and Nugent, K. A., "Quantitative phase-amplitude microscopy I: optical microscopy", Journal of Microscopy, Vol. 206, Pt 3, 194-203 (2002)

[7] Barty, A., Nugent, K. A., Pganin, D. and Roberts, A., "Quantitative optical phase microscopy", Opt Lett 23, 817-819 (1998)

[8] Dyer, P.E., Farley, R. J., and Giedl, R., "Analysis of grating formation with excimer laser irradiated phase masks", Opt. Comm., (115), 327-334 (1995)

[9] Xiong, Z., Peng, G. D., Wu, B. and P L Chu, "Effects of the Zeroth-Order Diffraction of a Phase Mask on Bragg Gratings", J. Lightwave Technol. 17, 2361- (1999)